A global, continental, and regional analysis of changes in extreme precipitation

Qiaohong Sun, Xuebin Zhang, Francis W. Zwiers, Seth Westra, & Lisa V. Alexander

2021

Original citation:

Sun, Q., Zhang, X., Zwiers, F. W., Westra, S., & Alexander, L. V. (2021). A global, continental, and regional analysis of changes in extreme precipitation. *Journal of Climate*, *34*(1), 243–258. https://doi.org/10.1175/JCLI-D-19-0892.1

A Global, Continental, and Regional Analysis of Changes in Extreme Precipitation

QIAOHONG SUN,[a] XUEBIN ZHANG,[b] FRANCIS ZWIERS,[a,c] SETH WESTRA,[d] AND LISA V. ALEXANDER[e,f]

[a] *Pacific Climate Impacts Consortium, University of Victoria, Victoria, British Columbia, Canada;* [b] *Climate Research Division, Environment and Climate Change Canada, Toronto, Ontario, Canada;* [c] *Nanjing University of Information Science and Technology, Nanjing, China;* [d] *School of Civil, Environmental and Mining Engineering, University of Adelaide, Adelaide, South Australia, Australia;* [e] *Climate Change Research Centre, University of New South Wales, Sydney, Australia;* [f] *Australian Research Council Centre of Excellence for Climate Extremes, Australia*

(Manuscript received 6 December 2019, in final form 6 August 2020)

ABSTRACT: This paper provides an updated analysis of observed changes in extreme precipitation using high-quality station data up to 2018. We examine changes in extreme precipitation represented by annual maxima of 1-day (Rx1day) and 5-day (Rx5day) precipitation accumulations at different spatial scales and attempt to address whether the signal in extreme precipitation has strengthened with several years of additional observations. Extreme precipitation has increased at about two-thirds of stations and the percentage of stations with significantly increasing trends is significantly larger than that can be expected by chance for the globe, continents including Asia, Europe, and North America, and regions including central North America, eastern North America, northern Central America, northern Europe, the Russian Far East, eastern central Asia, and East Asia. The percentage of stations with significantly decreasing trends is not different from that expected by chance. Fitting extreme precipitation to generalized extreme value distributions with global mean surface temperature (GMST) as a covariate reaffirms the statistically significant connections between extreme precipitation and temperature. The global median sensitivity, percentage change in extreme precipitation per 1 K increase in GMST is 6.6% (5.1% to 8.2%; 5%–95% confidence interval) for Rx1day and is slightly smaller at 5.7% (5.0% to 8.0%) for Rx5day. The comparison of results based on observations ending in 2018 with those from data ending in 2000–09 shows a consistent median rate of increase, but a larger percentage of stations with statistically significant increasing trends, indicating an increase in the detectability of extreme precipitation intensification, likely due to the use of longer records.

KEYWORDS: Extreme events; Precipitation; Climate change

1. Introduction

Long-term change in extreme precipitation has been the subject of extensive investigation based on a range of indices and detection methodologies. The annual maximum amount of precipitation accumulated over 1 day (Rx1day) or 5 consecutive days (Rx5day) are two important indices, representing extreme precipitation for moderate duration or more persistent events that often cause severe impacts on society. Long-term changes in these indices have been analyzed in numerous studies and various assessments of the Intergovernmental Panel on Climate Change (IPCC; e.g., IPCC 2012, 2013). These annual extremes have also been used to estimate the probability of rare events such as 100-yr return values, which are used in the design of infrastructure. Several previous studies have examined the trends in these annual precipitation statistics over global (Alexander et al. 2006; Asadieh and Krakauer 2015; Donat et al. 2013a,b; Westra et al. 2013) and Northern Hemisphere land areas (Groisman et al. 2005; Min et al. 2011; Zhang et al. 2013), different continents (Min et al. 2011; van den Besselaar et al. 2013), and in some regions (Barbero et al. 2017; Donat et al. 2016; Li et al. 2018). The IPCC Fifth Assessment Report concluded that "it is likely that since about 1950 the number of heavy precipitation events over land has increased in more regions than it has decreased" (Hartmann et al. 2013, p. 162). Extreme precipitation over land has intensified on average, with about two-thirds of stations showing increases in Rx1day (Groisman et al. 2005; Alexander et al. 2006; Donat et al. 2013b; Westra et al. 2013). Westra et al. (2013) estimated that the observed increase in Rx1day per 1 K increase in global mean surface temperature (GMST) ranged from 5.9% to 7.7% K^{-1}, which is close to the intensification expected from the Clausius–Clapeyron relationship (~7% K^{-1}; Boer 1993; Allen and Ingram 2002; O'Gorman 2015).

Most recent global studies of observed changes in extreme precipitation have used the HadEX2 dataset (Donat et al. 2013b) or its earlier version (Alexander et al. 2006), analyzing either station values (e.g., Westra et al. 2013) or gridded values (e.g., Donat et al. 2013b, Asadieh and Krakauer 2015). Some of these studies analyzed only Rx1day (e.g., Westra et al. 2013) while other studies examined more indices (e.g., Donat et al. 2013b). As HadEX2 ends in year 2010, it is important at the time of the IPCC Sixth Assessment to ask if the earlier results continue to hold and whether the climate change signal in extreme precipitation has strengthened given the additional precipitation observations and additional warming that has occurred over the past 9 years. It is also useful to ask if

Denotes content that is immediately available upon publication as open access.

Supplemental information related to this paper is available at the Journals Online website: https://doi.org/10.1175/JCLI-D-19-0892.s1.

Corresponding author: Qiaohong Sun, sunqh@uvic.ca

DOI: 10.1175/JCLI-D-19-0892.1

the changes in extreme precipitation are detectable at the regional scale.

To address these questions, here we first update the global analysis of observed changes in daily extreme precipitation of Westra et al. (2013), using the same methodologies but with additional recent observations. This provides a reference for comparison with the earlier study regarding the influence of the additional observations that have accumulated over the past nine years. Building on this, we then substantially expand the earlier study. One extension is to include Rx5day in our analysis as it provides an indication of the extremes of wet conditions persisting over several days that may be linked to widespread regional flooding and landslide disasters. Another important extension is to examine precipitation trends at different spatial scales including global, continental, and regional scales. As an updated version of HadEX2 was not available at the time of this analysis (although HadEX3 now exists; Dunn et al. 2020), we used a combination of station-based Rx1day and Rx5day data available from various sources that contributed to HadEX2, and Rx1day and Rx5day data from stations that were not available to HadEX2 such as a large collection of Chinese data. This approach is designed to provide as comprehensive a picture as possible of past changes in extreme precipitation over land areas from global to regional scales. As observations are lacking for many stations prior to the 1950s, we will report results for two periods, 1950–2018 and 1900–2018.

The paper is structured as follows: We describe the station data and analysis methods in section 2. The main results are presented in section 3. Conclusions are given in section 4.

2. Data and methods

a. Precipitation data

In this study we first assemble comprehensive up-to-date Rx1day and Rx5day datasets modeled after HadEX2. We started collecting and compiling Rx1day and Rx5day data from some of the main sources on which HadEX2 was based. These include the following: the European Climate Assessment Dataset (ECA&D; https://www.ecad.eu//dailydata/index.php; 1900–2018), Southeast Asian Climate Assessment and Dataset (SACA&D; http://sacad.database.bmkg.go.id/dailydata/index.php; 1900–2017), Latin American Climate Assessment and Dataset (LACA&D; http://lacad.ciifen.org/dailydata/index.php; van den Besselaar et al. 2015; 1900–2015), and GHCNDEX (Donat et al. 2013b) for the United States and India. Some of these records, notably those for India, end in the 1970s. We extract station data from these sources for the stations included in HadEX2, which represents the latest acquisition of high-quality station data around the globe. For example, in HadEX2, the subset of stations judged to be more likely to be free of discontinuities after 1950 caused by changes in station location were chosen for the United States by following the analysis by Peterson et al. (2008), who only selected National Weather Service cooperative and first-order weather observing sites with reasonably long records. Some HadEX2 data were also obtained from various regional data workshops (Aguilar et al. 2009; Caesar et al. 2011; Donat et al. 2014). If the station data are not updatable from the above data sources, we retained the data present in the HadEX2 dataset. Additionally, there were some data in HadEX2 that were not made publicly available due to data restrictions at the country of origin (e.g., Argentina). We therefore supplemented our data for Argentina by extracting 52 stations from the ETCCDI Climate Extreme Indices dataset (http://etccdi.pacificclimate.org/data.shtml).

Other stations used in this study are from the existing compiled and packaged datasets supplied by the national meteorological and hydrological services of their countries. We include the Adjusted and Homogenized Canadian Climate Data–Daily Temperature and Precipitation (Mekis and Vincent 2011), which includes adjusted daily precipitation for more than 460 Canadian locations. We use 840 Chinese stations available from the China Meteorological Administration, Russian data available from Russian Meteorological Service (http://meteo.ru/english/climate/d_temp.php), and Australian data from the Australian Bureau of Meteorology (http://www.bom.gov.au/climate/change/datasets/datasets.shtml). Data from the China Meteorological Administration have been tested for inhomogeneities and have been assessed for vigorous quality control to eliminate any spurious values. The Australian data are based on a historical rainfall dataset first documented in Lavery et al. (1992) that has been quality controlled by identifying and removing problematic records using statistical techniques, visual checks, and station history information. Since Rx1day and Rx5day values are not provided directly by these various sources, we used daily precipitation from these sources to calculate the indices, using the same criteria for the completeness of daily records used in the HadEX2 dataset. Thus, (monthly) index values were calculated only if no more than 3 daily observations were missing in a month and accordingly no more than 15 daily observations per year for the annual indices. If one or more of the monthly index values for a given year was missing, the corresponding annual index value was set to a missing value flag for that year. When sites from different sources overlapped, we retained those from the compiled and packaged datasets supplied by National Meteorological and Hydrological Services in preference to those from the ECA&D/SACA&D/LACA&D/GHCNDEX datasets since the former have been, at minimum, carefully quality controlled and in some cases adjusted to improve homogeneity.

Overall, we were able to collect Rx1day and Rx5day data from 14 796 land-based observing stations, with each station having at least 30 years of record during 1900–2018. Figure 1 shows a map of station locations classified by sources. The collection includes 5561 stations with data updated to year 2015 or later, which are mostly located in Canada, China, Europe, Russia, southeastern Australia, and the United States. Additionally, there are 8040 stations for which data availability stopped in 2009. Compared with Westra et al. (2013), who analyzed 8326 stations with more than 30 years of record over the period of 1900–2009, this represents a 75% increase in the total number of stations, resulting in improved spatial coverage including for Russia and China, which were sparsely sampled by the earlier study. There is, however, little improvement over most of Africa, South America, and West Asia, where spatial coverage of stations is still very poor. In addition, prior to 1950 most

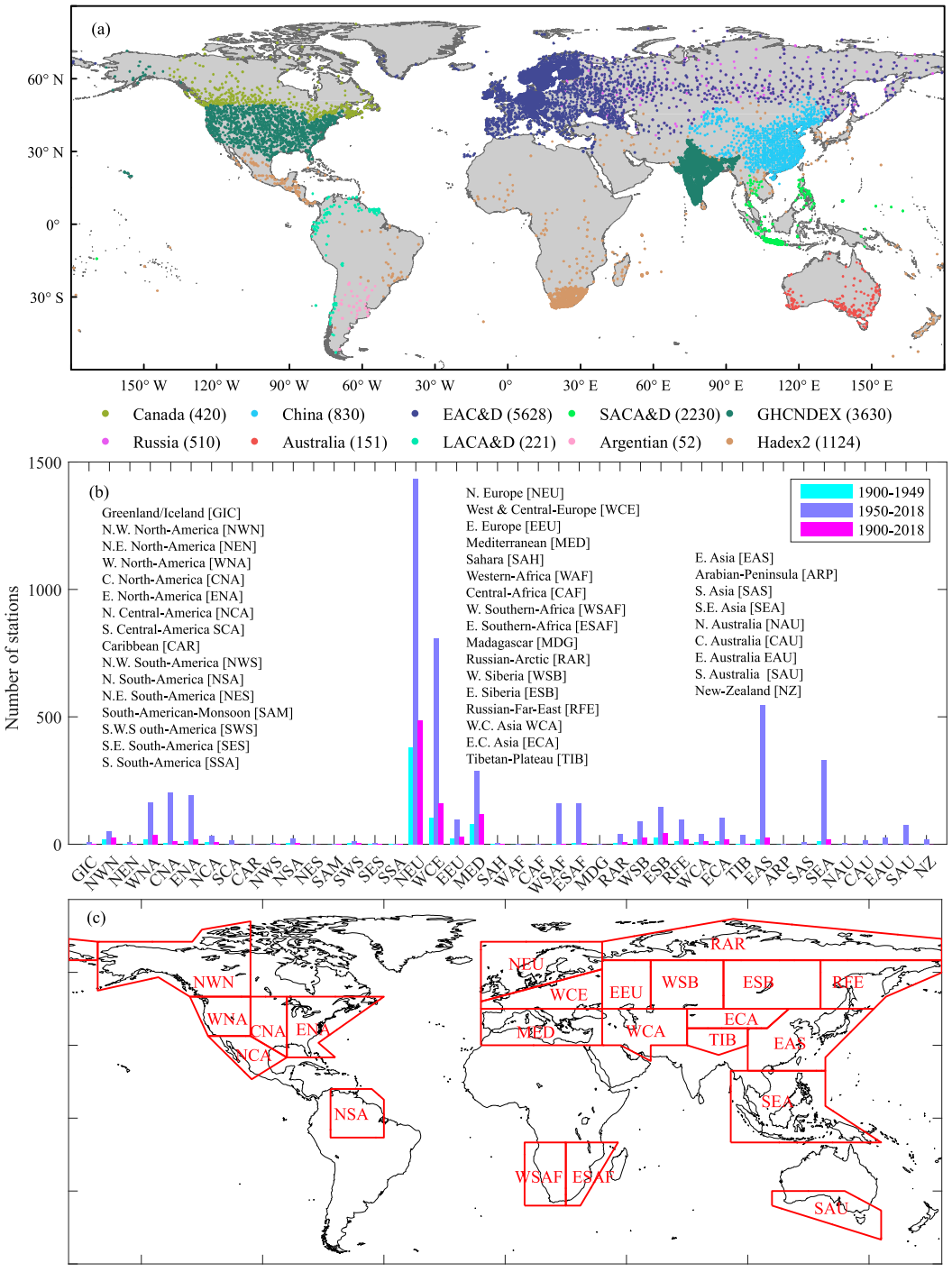

FIG. 1. Locations of stations and IPCC6 regions available for this study. (a) Sources of station observations. The colored dots represent the different data sources that are described in the main text. (b) Number of stations that have less than 30% missing Rx1day and Rx5day values for each period and each IPCC AR6 reference region. (c) IPCC AR6 reference regions with more than 30 stations that have less than 30% missing Rx1day and Rx5day values during the 1950–2018 period. There are 18 such regions.

station records are confined to North America, Europe, South Asia, the Amazon, and Australia. The number of stations increased notably after the 1950s (Fig. 1b), with 12 323 stations having at least 30 years of record during 1950–2018. The Westra et al. (2013) results based on stations with at least 30 years record during 1900–2009 were heavily weighted to changes since the 1950s rather than the whole century, although they found consistent results when using smaller

subsets of stations with at least 50 and 70 years of record over the same time window. For these reasons, we will analyze two periods, one starting from 1950 and another covering the whole period.

We restrict our analyses to stations that have at least 70% of the annual Rx1day/Rx5day data within the corresponding period (at least 48 and 83 years for the 1950–2018 and 1900–2018 periods, respectively). In practice, this 70% lower bound for temporal completeness results in a collection of stations for which the median level of temporal completeness is about 85%. This is important, because the power of the trend detection test is reduced when records are shorter. A total of 7293 and 1974 stations, respectively, met the 70% completeness criterion for these two periods.

The completeness criterion represents a trade-off between the power of the trend detection tests we use and spatial coverage. A higher requirement for temporal completeness would result in a substantial reduction of spatial coverage, with the number of complete stations for 1950–2018 dropping to only 855 if we were to require 100% complete records. We have subsampled the 855 complete records in various ways to mimic how data might be missing to evaluate the impact of records with different proportions of missing years, and different placements of those years within the record, on the power of trend detection and our estimates of the sensitivity of extreme precipitation to warming (see details in Figs. S1 and S2 in the online supplemental material). We find, not surprisingly, that the rate at which significant intensification is detected is reduced when records contain fewer years. On the other hand, our sensitivity estimates are not largely affected by missing data, but may become more uncertain when records contain few years and all stations have the same missing data profile.

To enable comparison between results presented here and those of Westra et al. (2013), we also analyzed the data for the stations with at least 30 annual maxima, and present the results in the online supplemental material. In addition, we also conduct a comprehensive analysis over different spatial domains including the global land, continents, and regions used in the IPCC WGI Sixth Assessment Report (Iturbide et al. 2020). For this purpose, we select 22 regions with more than 30 stations that have at least 70% of the annual Rx1day and Rx5day values during the 1950–2018 period (Fig. 1c).

b. Methods

We use two well-established methodologies that were employed by Westra et al. (2013). These include the estimation of the long-term trend in extreme precipitation and its statistical significance based on nonparametric methods, and quantification of the relationship between extreme precipitation and GMST by fitting generalized extreme value (GEV) distributions to the annual extremes of precipitation with GMST as a covariate. For the latter, we use the GMST of the National Aeronautics and Space Administration (NASA) Goddard Institute for Space Studies (GISS) (Hansen et al. 2010) expressed as temperature anomalies relative to the 1951–80 mean. These methods are applied to station data separately. Field significance for a region is established using the bootstrap method of Livezey and Chen (1983). These methods are briefly summarized below; more details can be found in Westra et al. (2013).

First, we use the nonparametric Mann–Kendall test (Mann 1945) to identify statistically significant trends in the Rx1day and Rx5day series. The null hypothesis when applying the Mann–Kendall test is that the data are independent and identically distributed (iid). The actual significance level of the test can differ substantially from the nominal level that is specified when data are serially dependent, in which case the data can be prewhitened before applying the test (e.g., Zhang and Zwiers 2004). Westra et al. (2013), however, showed that serial dependence is weak in annual maximum precipitation across all global stations, and thus we have not applied a prewhitening procedure in this study. The test is two-sided, and a trend is considered to be statistically significant if it is significant at the 5% level. Stations are classified as having "significant increasing," "significant decreasing," or "non-significant" trends depending on the sign and the absolute value of the test statistic.

Second, the nonstationary GEV distribution is used to quantify the precipitation-temperature relationship. The cumulative distribution function for a GEV distributed random variable Z has the following form:

$$G(\mathsf{Z}) = \begin{cases} \exp\left\{-\left[1+\xi\left(\dfrac{\mathsf{Z}-\mu}{\sigma}\right)\right]^{-1/\xi}\right\} & \text{when} \quad \xi>0, z>\mu-\dfrac{\sigma}{\xi} \quad \text{or} \quad \xi<0, z<\mu-\dfrac{\sigma}{\xi} \\ \exp\left[-\exp\left(-\dfrac{z-\mu}{\sigma}\right)\right] & \text{when} \quad \xi=0, z\in R \end{cases}, \tag{1}$$

where μ, σ, and ξ are the location, scale, and shape parameters, respectively. The distribution can be made nonstationary, by making one or more of the parameters functions of a covariate. We would like to examine whether the distributions of the annual maxima are changing with GMST change. Thus, we fit station Rx1day or Rx5day series to nonstationary GEV distributions separately, with the location parameter of the distributions μ being a linear function of GMST:

$$\mu = \beta_0 + \beta_1 T, \tag{2}$$

where T is the GMST anomaly and β_0 and β_1 are the intercept and slope coefficients. Previous studies have suggested the location-only model is sufficient when considering the precipitation–temperature relation in observations, with similar results derived from a time-varying scale parameter model (Westra et al. 2013). The method of the maximum likelihood is used to estimate the parameters. The statistical significance of this relationship is inferred with the likelihood ratio test at the 5% level. We classify stations as having significant positive association, significant negative association, or non-significant

association with the GMST series depending the sign of the slope coefficient and the value of the likelihood ratio test statistic.

The percentage change in annual extreme precipitation per 1 K of GMST increase is estimated with the fitted GEV distributions and interpreted as an estimate of the sensitivity of extreme precipitation to GMST change. This is achieved by considering how the median of the fitted distribution, which corresponds to the 2-yr return value, changes conditional on temperature anomalies of 1 and 0 K from the fitted nonstationary GEV distributions and interpreting the ratio between the two values as a scaling estimate. Since the pth quantile of the GEV distribution is given by $\mu + \sigma\{[-\ln(p)]^{-\xi} - 1\}/\xi$, where the location parameter μ is given by Eq. (2), it is easily seen that the sensitivity of the median to 1 K of warming is given by $[\beta_1/(\beta_0 + \sigma\{[-\ln(p)]^{-\xi} - 1\}/\xi)] \times 100\%$.

We estimated the uncertainty of the sensitivity value using a resampling method. We selected n years ($n = 69$ for the 1950–2018 period, $n = 119$ for the 1900–2018 period) at random with replacement, and fitted the nonstationary GEV models using the precipitation extremes and temperatures appropriate to the years selected, which preserves the connection between extremes and temperature. Then, we estimated the sensitivity from the fitted models. Resampling was performed 1000 times to develop a sampling distribution for the sensitivity, which was used to estimate a 5%–95% confidence interval for the sensitivity value. Some studies suggested using a block bootstrapping approach with a block size of two or three, to account for autocorrelation effects (e.g., Alexander et al. 2006; Kiktev et al. 2003). We compared the outcome of the conventional spatial bootstrap procedure and the 2-yr block bootstrap. The results are similar. For this reason, we only report results based on the conventional spatial bootstrap procedure. In addition, we use latitudinal temperature change to adjust local sensitivity values to ensure that reported sensitivities correspond to latitudinal temperature changes.

Third, the field significance for the ensemble of test results obtained from all stations was assessed using the method of Livezey and Chen (1983) in order to avoid "false discovery." All statistical tests are designed to have a specified false discovery rate (i.e., type I error rate) when the null hypothesis is true, which is given by the stated significance level. When a 5% significance level is set, we should expect rejection of the null hypothesis to occur, on average, at 5% of locations when the null hypothesis is true. The Livezey and Chen procedure is used to determine whether there is evidence that the null hypothesis is being rejected at more locations than would be consistent with the specified false discovery rate. The procedure does this taking the effects of the spatial correlation between test results into account. Field significance can be evaluated for the whole global land area, or a continent or a region. This procedure involves shuffling the spatial fields of extreme precipitation by year such that data for the same year in the observation for all stations are kept in the same year in the shuffled series to retain the spatial dependence. Temperature, however, is not reshuffled, thereby breaking any connection between extreme precipitation and temperature. After each reshuffling, trends are computed and tested for statistical significance for both the nonparametric and GEV-based approaches. The bootstrap sampling is conducted 1000 times. The statistics such as the percentage of stations with significant trends are used to construct the probability distribution for those statistics. A particular statistic computed from the original unshuffled data that lies above the 95th percentile of statistics from the bootstrap sample is considered to be field significant at the 5% significance level.

3. Results

a. Changes in extreme precipitation since 1950s

1) GLOBAL SCALE

Figure 2 shows the maps of Rx1day and Rx5day trends along with the proportion of stations with a significant positive or negative trend for 1950–2018 and the bootstrap distribution of this proportion when the link between time and the observed sequence of annual maxima is broken. Overall, trends over the space are very noisy with widely scattered increasing and decreasing trends. This is consistent with the Li et al. (2019) finding that a well-constrained estimate of changes in extreme precipitation is difficult to obtain with individual records of limited length and a relatively weak signal compared to background year-to-year variability. There are important patterns, however. There are many more stations showing increasing than decreasing trends, with about two-thirds (66%) of stations showing increasing trends and close to one-third (34%) showing decreasing trends in Rx1day. This result is very close to the findings in previous studies using HadEX2 station data (Westra et al. 2013) or gridded values (Min et al. 2011). Furthermore, 9.1% of stations show a statistically significant increasing trend, which is much higher than could be expected from random chance alone, as it is far outside of the simulated bootstrap distribution when the link between time and extreme precipitation is broken (indicated by the blue bars in Fig. 2b). In contrast, the percentage of stations showing a statistically significant decreasing trend is only about 2.1%, comparable with what one would expect from random chance (Fig. 2c). This means that at the global scale, there is indeed a detectable increase in Rx1day. Although the spatial distribution of stations with significant increasing trend is largely random, there is slightly higher concentration in eastern North America, Europe, and South Africa. It is also noted that even though stations with significantly decreasing trends are largely randomly distributed over space, there are a few relatively well-organized areas where the intensity of extreme precipitation seems to be weakening, such as the Canadian Prairies, some parts of the western United States, Australia, and northern China.

Results for Rx5day are very similar to those for Rx1day, with a larger percentage of stations (10.9%) showing statistically significant increasing trends, which is again highly field significant. Of all the stations, about 5% show statistically significant increasing trends for both Rx1day and Rx5day. About 2.3% of stations have statistically significant negative trends in Rx5day, consistent with what one would expect from random chance.

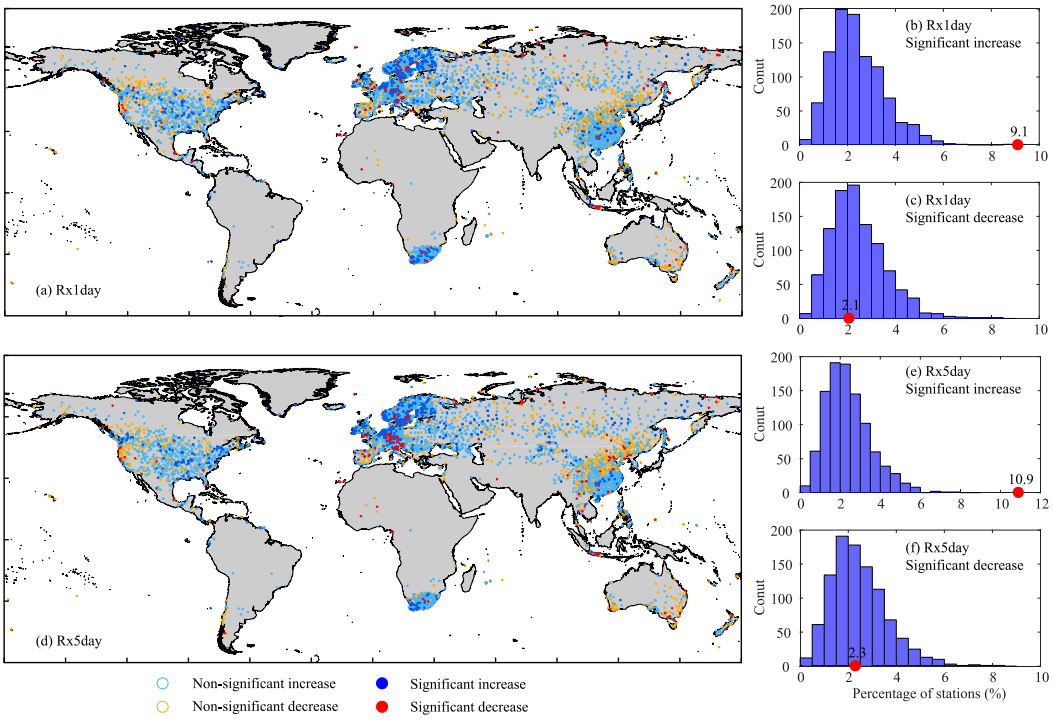

FIG. 2. Summary of Mann–Kendall trend analyses for the period 1950–2018 for 7293 stations. (a),(d) Maps of locations of stations with trends for Rx1day and Rx5day, respectively. Light blue open dots indicate non-significant increasing trends and light red open dots mark non-significant decreasing trends. Dark blue and red filled dots indicate statistically significant trends as determined by a two-sided test conducted at the 5% level. (b),(c),(e),(f) Percentage of stations with statistically significant increasing and decreasing trends. The histogram represents the distribution of percentage of stations with significant trends from 1000 bootstrap realizations when the connection between time and the occurrence of annual extremes is broken. The red dots represent the values from the observational data.

2) RELATIONSHIP WITH GLOBAL MEAN SURFACE TEMPERATURE

Figure 3 provides maps of local extreme precipitation sensitivity to global warming along with global median sensitivity based on the GEV fitting. About two-thirds (68%) of stations show an increase in Rx1day with warming while the remaining stations show a decrease. The percentage of stations showing a significant positive relation, at 11.6%, is significantly higher than what would be expected from random chance alone, while the percentage of stations showing a significant negative relation is only about 2.4%, consistent with expectations from random chance. Taking all stations together, the median percentage Rx1day increase is about 6.6% per 1 K of GMST increase (5.1% to 8.2% K^{-1}; 5%–95% confidence interval). This value is comparable to that of Westra et al. (2013). Results for Rx5day are similar to Rx1day except the precipitation sensitivity is slightly smaller at 5.7% K^{-1} (5.0% to 8.0% K^{-1}). As global land warms faster than GMST, precipitation sensitivity is thus smaller than what may be expected from the Clausius–Clapeyron relation when scaled with land temperature change, although a detailed comparison between global sensitivity and local sensitivity is outside of the scope of this analysis.

To reduce the influence of the uneven geographic distribution of stations, we adopted the area-weighted average method suggested in Westra et al. (2013) to calculate a revised estimate of the sensitivity of Rx1day and Rx5day to GMST. The global land area is divided into 1° × 1° latitude–longitude grid boxes. Within each grid box, the mean of the sensitivity values obtained at all stations within that grid box is calculated. An area-weighted global average sensitivity is then calculated from the grid box averages. The revised global land sensitivity values, which are slightly lower than their unweighted counterparts, are 6.1% and 5.4% K^{-1} for Rx1day and Rx5day, respectively. Evidence from climate models suggests that these numbers (either weighted or unweighted) should be roughly representative of global land areas despite incomplete land coverage. In particular, Kharin et al. (2013) calculated sensitivities of 20-yr return levels of extreme precipitation to warming from CMIP5 (see Figs. 5 and 6 in their paper) and obtained sensitivities that are relatively uniform over land. Overlaying the locations of the stations used in this study on their map of estimated sensitivities suggests that the available observing network configuration roughly samples land areas where sensitivities are representative of typical values for global land areas.

3) CONTINENTAL SCALE

Figure 4 shows the percentage of station with significant positive or negative trends during the 1950–2018 period over six continents. The percentage of stations with significant

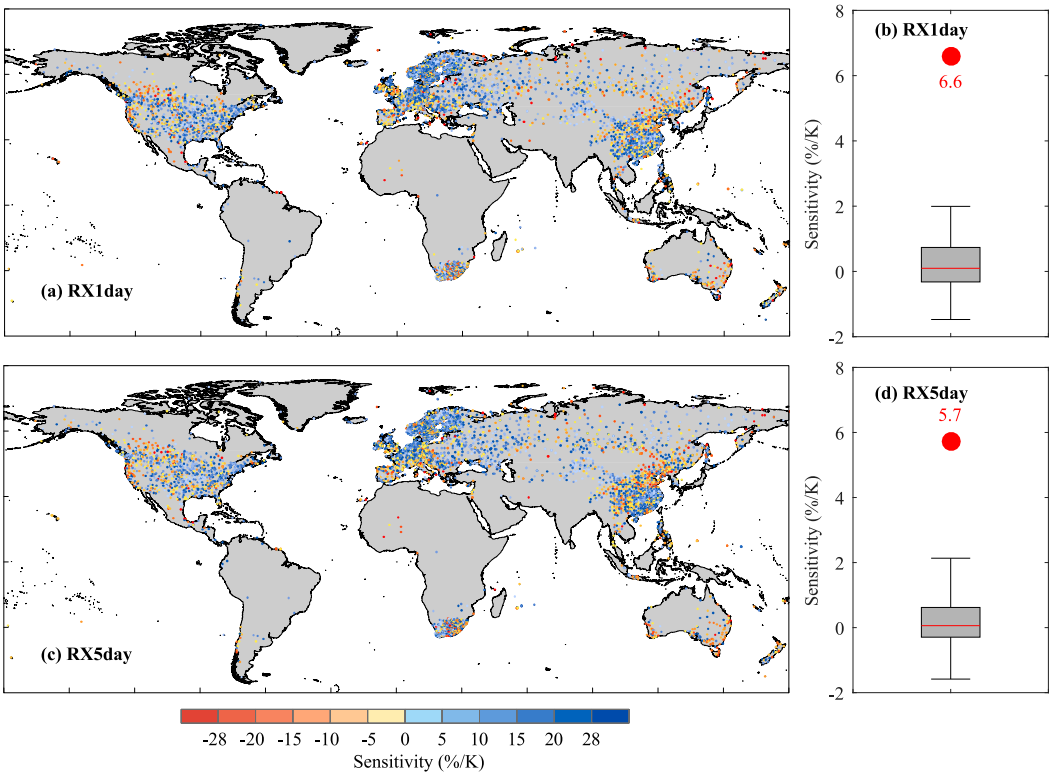

FIG. 3. Estimated local sensitivity of precipitation extremes to temperature change (percentage change per 1 K increase in global mean surface temperature) during the period 1950–2018 for (a),(b) Rx1day and (c),(d) Rx5day. The red dots in (b) and (d) represent median sensitivity among global land-based observing stations while the box-and-whisker plots summarizes the breadth of the estimated distribution of the sensitivity from 1000 bootstrap realizations under conditions when the null hypothesis that the sensitivity is zero is true (i.e., the resampling process has broken the link between temperature and precipitation). In these plots, the 25th and 75th percentiles are shown as lower and upper edges of the boxes while the median is marked by the center line. The upper and lower whiskers show the 97.5th and the 2.5th percentiles. The observed median sensitivity estimate is evidently significantly larger than zero.

negative trends is not field significant for both Rx1day and Rx5day in all continents. The evidence for intensification is field significant in the well-gauged continental domains (Asia, Europe, and North America) but not in Africa, South America, and Australasia (including Australia and New Zealand). As also detailed in the following paragraphs, increasing trends in Rx1day and Rx5day can be detected in all continents except Australasia.

Europe has the highest station density used in our analysis with 3510 stations. The fraction of stations exhibiting positive trends is also largest among all continents at about 70% in Rx1day. Among them, there are about 10.6% of stations showing significant positive trends, mostly located in northern and central Europe where a higher station density can be found. Only 1.3% of stations have significant negative trends, and these are distributed quite randomly over Europe. These results are in general agreement with previous European-wide studies (e.g., Zolina 2012; van den Besselaar et al. 2013) and some national studies (e.g., Blöschl et al. 2012; Zolina 2012; Jones et al. 2013) of changes is daily precipitation in which an increase in extreme winter precipitation over Europe and an increase in extreme autumn, winter, and spring precipitation in northern Europe were found. Results for Rx5day are similar to those for Rx1day, except the percentages of stations with increases and with significant trends are both slightly higher.

Asia has a second highest number of gauges, being represented by 1684 stations in our study. The fractions of stations showing increasing trends and statistically significant increasing trends are 60% and 7.2%, respectively, with increases mainly located in southern China and Russia. About 40% of stations show a downward trend, mostly in northern China. The percentage of stations showing significant positive trends in Rx5day is close to that for Rx1day. The percentage of stations with significantly increasing trends lies outside the 95% uncertainty range determined with the 1000 bootstrap realizations under the no-trend hypothesis for both Rx1day and Rx5day (Fig. 4), implying that an overall increasing trend in extreme precipitation can be detected. Note that it is more difficult to detect significant increases (or decreases) at smaller spatial scales. For instance, Li et al. (2018) found that fractions of significant increase or decrease in Rx1day in Chinese stations are both within the 95% uncertainty range when a similar method was used. Note that Indian data in GHCN-Daily mostly end in the early 1970s; thus, trends for India cannot be updated this point.

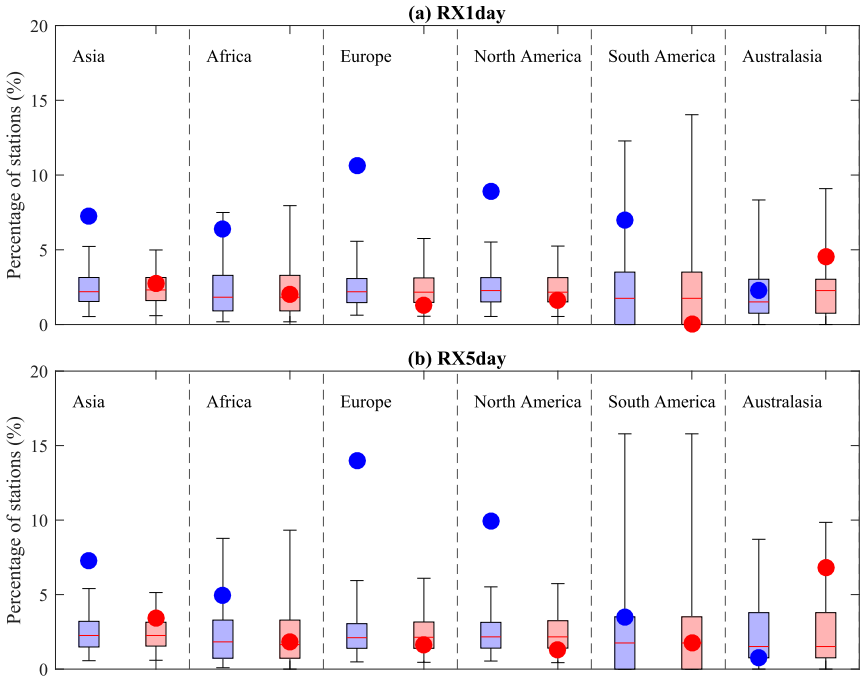

FIG. 4. Continental summaries of the percentage of stations with statistically significant trends (according to the Mann–Kendall trend test) in extreme precipitation for 1950–2018. The blue and red colors indicate significant positive and negative trends, respectively. Dots indicate percentages estimated from the observations. Box-and-whisker plots summarize the breadth of the distribution from 1000 bootstrap realizations under the no-trend null hypothesis. In the plots, the 25th and 75th percentiles are shown as lower and upper edges of the boxes while the median is marked by the center red line. The upper and lower whiskers show the 97.5th and the 2.5th percentiles, respectively.

The results for North America are similar to those for Asia and Europe, again showing that extreme precipitation has increased in many more locations than where it has decreased in both Rx1day and Rx5day. These results are also consistent with earlier studies (e.g., Barbero et al. 2017), which analyzed changes in extreme precipitation at 733 North American stations for the period from 1950 to 2011. The similarity of our results with those of Barbero et al. (2017) indicates intensification of daily precipitation extremes is robust to differences in sample size.

The spatial coverage of stations over Africa and South America is poor and uneven, making it difficult to infer whether there is an overall significant increasing trend in extreme precipitation in these two continents. Nevertheless, more than 64% of stations available in these continents show positive trends.

Australasia is distinct from other continents in that, among available stations, more stations show negative trends than positive trends for both Rx1day and Rx5day. Stations with decreasing trends are mainly located in southwestern and southeastern Australia (Figs. 1a,c). The fraction of stations with significant decreases are 4.5% for Rx1day and 6.8% for Rx5day. This is consistent with previous studies that suggested a decrease in extreme precipitation in southwest Western Australia, southeastern Australia, and southeast Queensland (Dey et al. 2019). Some of the causes of the observed decrease in the intensity of precipitation extremes in these regions have been linked to changes in circulation, including the southward shift in the subtropical ridge due to Hadley cell expansion (Timbal and Drosdowsky 2013; Whan et al. 2014), external forcing induced reduction in the number of synoptic systems (Hope 2006; Raut et al. 2014; Dey et al. 2019), or changes in the southern annular mode due to ozone depletion over Antarctica and increasing GHGs (Cai et al. 2011; Thompson et al. 2011). However, note that other parts of Australia (e.g., the northwest) have seen observed increases in extreme rainfall including Rx1day (e.g., Alexander and Arblaster 2017). Also, Alexander and Arblaster (2017) and Contractor et al. (2018) found evidence of an overall intensification of Rx1day for Australia as a whole. For example, Alexander and Arblaster (2017) looked into trends in Rx1day and Rx5day averaged over Australia (their Table 3 and Fig. 4 for time series) and found increasing Rx1day trends over the period 1911–2010. This somewhat contradicts the findings here but it should be noted that the stations included in this study are primarily located in the regions (southern Australia) where most of the declines in extreme precipitation have been detected. Results for Australia are sensitive to the choice of indices, time period, and dataset used and are heavily affected low-frequency modes of variability such as ENSO/IPO (e.g., King et al. 2013), which makes trend estimation substantially more uncertain. Therefore, some care is required when interpreting the results from this study as ''Australia-wide.''

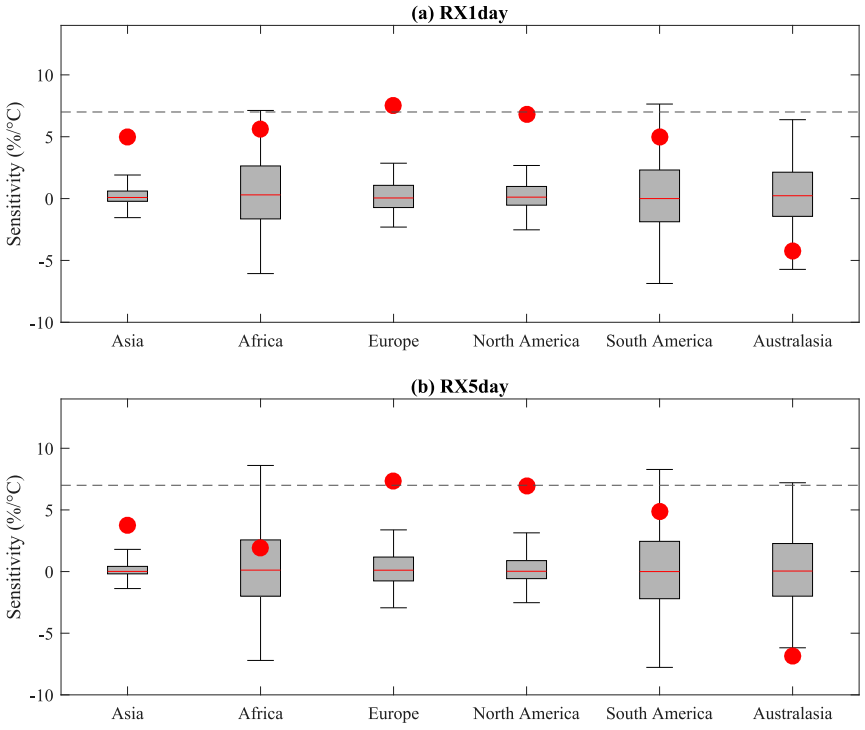

FIG. 5. Continental summaries of sensitivity of extreme precipitation per 1 K increase in global mean surface temperature for 1950–2018. The red dots indicate the median of local sensitivities estimated at stations within each continent. The box-and-whisker plots summarizes the breadth of the distribution from 1000 bootstrap realizations under the zero sensitivity hypothesis. In these plots, the 25th and 75th percentiles are shown as lower and upper edges of the boxes while the median is marked by the center red line; the upper and lower whiskers show the 97.5th and the 2.5th percentiles, respectively. The horizontal dashed line shows the nominal Clausius–Clapeyron rate of 7% K^{-1} for reference.

Figure 5 displays continental summaries of changes in Rx1day and Rx5day, expressed as percentage change per 1 K GMST increase, as estimated by fitting GEV distribution to precipitation data with GMST as a covariate. Results indicate significant intensification of extreme precipitation with warming over continents where sufficient data are available to make confident assessments (i.e., Europe, Asia, and North America). The median sensitivities over these continents for both Rx1day and Rx5day are significantly greater than zero, with median values close to ~7% K^{-1} warming in GMST in Europe and North America, and values that are somewhat smaller in Asia. The sensitivity has a wider spread from bootstrap samples over regions with poor spatial coverage including Africa, South America, and Australasia. Based on available data, sensitivities to warming appear to be positive in Africa and South America, and negative in Australasia.

4) REGIONAL SCALE

Table 1 summarizes trend analysis results for Rx1day and Rx5day over 22 of 45 land regions used in the IPCC WGI Sixth Assessment Report that contain at least 30 stations that satisfy our data completeness criteria. Almost all regions have a higher fraction of stations with positive trends than that with negative trends for Rx1day, except for northwestern North America, the Russian Arctic, and southern Australia. Further, statistically significant intensification in Rx1day is found in seven regions, comprising central North America, eastern North America, northern Central America, northern Europe, the Russian Far East, east central Asia, and East Asia, with the percentages of stations with significant increases being higher than would be expected in a stationary climate. It should be noted that the percentages of stations with significantly increasing and significantly decreasing trends are both higher than would be expected in a stationary climate in the Russian Arctic. The results for Rx5day are similar except that night regions (two more than Rx1day) showed statistically significant intensification. These results indicate again that the intensification of extreme precipitation is widespread since the 1950s, occurring over almost all observed regions based on the data used in this study.

Regional results for GEV modeling analysis are listed in Table 2. Overall, Rx1day and Rx5day have intensified significantly with warming over 10 and 8 regions, respectively, although extreme precipitation decreases with warming in the South Australia region. Donat et al. (2016) showed that Rx1day averaged over both dry and wet regimes increases with global surface temperature change in both observations and climate models. The dominant increasing trends over dry

TABLE 1. Percentage of stations with increasing, decreasing, statistically significant increasing, and statistically significant decreasing trends in Rx1day and Rx5day based on the Mann–Kendall test over the IPCC AR6 reference regions (Iturbide et al. 2020) during the 1950–2018 period. Values higher than the upper 97.5th percentile from the 1000 bootstrap realizations under the no-trend null hypothesis are shown in boldface. There are no regions in which the percentage values lie below the lower 2.5th percentile of these bootstrap distributions.

		Rx1day				Rx5day			
Reference regions	No. of stations	Increase (%)	Decrease (%)	Significant increase (%)	Significant decrease (%)	Increase (%)	Decrease (%)	Significant increase (%)	Significant decrease (%)
Northwest North America (NWN)	89	43.8	56.2	3.4	4.5	55.1	44.9	**9.0**	2.2
Western North America (WNA)	218	60.6	39.4	4.6	2.8	53.7	46.3	5.5	3.2
Central North America (CNA)	270	**74.8**	25.2	**12.2**	0.7	**75.6**	24.4	**11.5**	0.0
Eastern North America (ENA)	269	**72.9**	27.1	**9.3**	0.4	**79.2**	20.8	**13.4**	0.7
Northern Central America (NCA)	44	61.4	38.6	**11.4**	0.0	61.4	38.6	9.1	0.0
Northern South America (NSA)	39	64.1	35.9	2.6	0.0	82.1	17.9	2.6	0.0
Northern Europe (NEU)	1988	**76.1**	23.9	**14.4**	1.2	**79.9**	20.1	**18.4**	1.1
Western and central Europe (WCE)	1236	65.0	35.0	6.6	1.1	63.0	37.0	**10.0**	2.1
Eastern Europe (EEU)	163	**73.6**	26.4	7.4	1.8	**79.1**	20.9	**14.7**	0.6
Mediterranean (MED)	343	54.2	45.8	4.7	3.8	50.7	49.3	4.4	5.5
West Southern Africa (WSAF)	249	**66.3**	33.7	8.0	1.2	65.9	34.1	8.8	0.8
East Southern Africa (ESAF)	279	64.9	35.1	5.7	1.1	54.5	45.5	2.2	0.7
Russian Arctic (RAR)	95	48.4	51.6	**11.6**	**17.9**	55.8	44.2	**14.7**	**15.8**
Western Siberia (WSB)	146	**73.3**	26.7	7.5	1.4	65.8	34.2	**11.6**	0.0
Eastern Siberia (ESB)	215	59.1	40.9	5.6	0.9	58.6	41.4	7.0	1.4
Russian Far East (RFE)	131	56.5	43.5	**11.5**	6.9	64.1	35.9	**12.2**	2.3
Western central Asia (WCA)	53	64.2	35.8	7.5	0.0	**83.0**	17.0	3.8	0.0
Eastern central Asia (ECA)	106	72.6	27.4	**12.3**	0.0	71.7	28.3	**12.3**	0.9
Tibetan Plateau (TIB)	37	59.5	40.5	5.4	2.7	64.9	35.1	5.4	2.7
East Asia (EAS)	599	59.9	40.1	**5.5**	1.2	53.3	46.7	3.7	3.3
Southeast Asia (SEA)	412	55.6	44.4	7.8	4.1	65.8	34.2	8.3	4.4
Southern Australia (SAU)	75	44.0	56.0	4.0	2.7	30.7	69.3	0.0	9.3

regions do not change since other arid/semiarid regions, such as eastern and western Siberia, western and eastern central Asia, and the Tibetan Plateau, show positive sensitivity value. Overall, results are generally similar to those for long-term trends as summarized in Table 1, although the magnitude of sensitivity varies widely. Different factors may have contributed to the wide sensitivity range, especially for large sensitivity values. These include possible regional forcing differences, circulation changes that may or may not be due to an anthropogenic influence, and, likely most importantly, differences between the regional and global warming rates. In addition, sampling variability is expected to be much higher at the regional scale, and this is also likely to contribute to the wider sensitivity range. The sensitivity in the northern high latitudes becomes much smaller if changes in precipitation are scaled with latitudinal temperature change since temperature changes in the

TABLE 2. Percentage of stations with statistically significant positive or negative association between extreme precipitation (Rx1day and Rx5day) and global mean surface temperature (GMST), and the median sensitivity of extreme precipitation to a 1 K increase in GMST for IPCC AR6 reference regions during the 1950–2018 period. Values significant at the 5% level are shown in boldface.

	Rx1day			Rx5day		
Region name	Significant positive (%)	Significant negative (%)	Sensitivity (% K^{-1})	Significant positive (%)	Significant negative (%)	Sensitivity (% K^{-1})
Northwest North America (NWN)	6.7	4.5	−1.9	**12.4**	0.0	0.1
Western North America (WNA)	7.3	2.3	**5.5**	6.0	0.9	5.4
Central North America (CNA)	**14.1**	1.1	**8.7**	**13.0**	0.4	**9.9**
Eastern North America (ENA)	**9.3**	0.0	**8.7**	**13.4**	0.7	**7.9**
Northern Central America (NCA)	2.3	4.5	1.0	6.8	2.3	−1.6
Northern South America (NSA)	0.0	2.6	0.2	0.0	2.6	2.9
Northern Europe (NEU)	**16.5**	1.4	**8.8**	**20.6**	1.2	**9.3**
Western and central Europe (WCE)	**12.1**	1.1	**5.9**	**14.5**	1.5	**5.5**
Eastern Europe (EEU)	**17.8**	1.2	**13.0**	**18.4**	0.0	**12.1**
Mediterranean (MED)	5.2	4.7	2.3	2.0	7.3	−2.6
West southern Africa (WSAF)	**12.9**	2.8	**9.5**	6.8	2.0	8.7
East southern Africa (ESAF)	5.4	2.5	2.8	3.6	2.5	−0.4
Russian Arctic (RAR)	**11.6**	**14.7**	**4.8**	**14.7**	**12.6**	**10.0**
Western Siberia (WSB)	8.2	0.7	**8.0**	**11.0**	0.7	**9.3**
Eastern Siberia (ESB)	**8.8**	2.3	4.1	7.4	3.3	2.6
Russian Far East (RFE)	6.9	6.9	3.8	**9.9**	3.1	4.9
Western central Asia (WCA)	3.8	3.8	2.7	9.4	0.0	**7.8**
Eastern central Asia (ECA)	**13.2**	0.0	**17.2**	**13.2**	0.0	**14.0**
Tibetan Plateau (TIB)	8.1	0.0	1.3	10.8	5.4	3.5
East Asia (EAS)	**7.7**	1.3	**5.5**	3.8	2.7	1.4
Southeast Asia (SEA)	**11.9**	7.0	3.2	8.0	4.9	3.8
Southern Australia (SAU)	1.3	5.3	−2.2	1.3	6.7	**-8.3**

high northern latitudes are larger than global mean temperature changes. This does raise a question regarding which temperature—global, regional, or local temperature—to use when discussing extreme precipitation sensitivity at the regional scale. Exactly what temperature to use to satisfactorily approximate the change in saturation vapor pressure with temperature under nonideal conditions is far from clear. Several previous studies summarizing and assessing observed or projected changes in extreme precipitation at a global scale have used GMST, and thus for comparability as well as its policy relevance (IPCC 2018) we do so here as well.

b. Changes in extreme precipitation in longer records

Figure 6 displays the percentage of land-based stations globally with significant trends in relation to sample size. Figure 6a and Table 3 shows results for the 1900–2018 period using 1974 stations that have at least 70% of the annual Rx1day and Rx5day data. These long-term stations are located mainly in the Northern Hemisphere midlatitudes and parts of Australia and South Africa (Fig. S3). It is clear that extreme precipitation has increased over the region with data coverage. Overall, extreme precipitation has increased in many more regions than where it has decreased, for both Rx1day and Rx5day. The fraction of stations showing an increasing trend is greater than 70% for both Rx1day and Rx5day, and the fraction of stations with significant increasing trends is 17.1% and 23.0% for Rx1day and Rx5day, respectively. These fractions are roughly double the corresponding fractions of the same collection of stations when only data for 1950–2018 are used (Fig. 6a). The fractions are also larger when at regional scales (Table 3; see also Table S1). These large differences in the proportion of stations with significant increase between the two periods is unlikely due to the difference in spatial coverage of the stations. Over the regions where long-term observations exist, stations with significant trends are also quite evenly distributed.

The percentage of stations with significant increases is also much larger than that obtained from analysis using stations

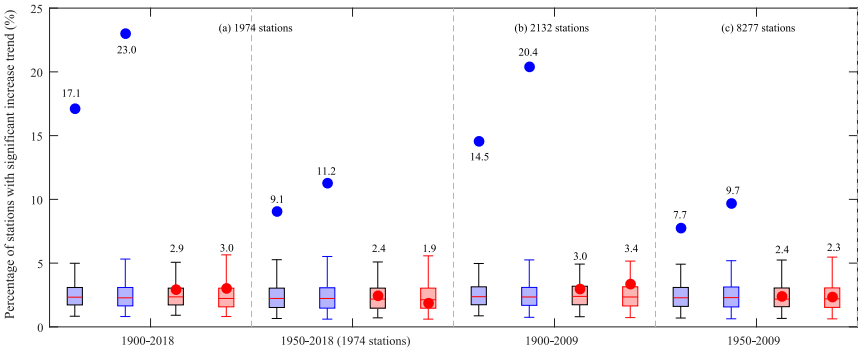

FIG. 6. Summaries of the percentage of stations with statistically significant trends in extreme precipitation for different datasets and different periods. Results are shown for subsets of stations that have less than 30% missing values during (a) 1900–2018, (c) 1900–2009, and (c) 1950–2009, respectively. Blue and red dots indicate the percentage of significant positive and negative trends, respectively. The box-and-whisker plots summarize the breadth of the distribution from 1000 bootstrap realizations under the no trend null hypothesis. These plots show the 25th and 75th percentiles as the lower and upper edges of the boxes while the median is marked by the center red line. The upper and lower whiskers show the 97.5th and the 2.5th percentiles, respectively.

with more than 30 years of data (Figs. S4 and S5) as was done in Westra et al. (2013). The station selection criterion allowing stations with records as short as 30 years would have resulted in a predominance of information from trend tests based on shorter records with a shorter median length of record; such tests are inherently less powerful than tests based on longer records. On the other hand, the percentage of stations with significant negative trends is unchanged, remaining consistent

TABLE 3. Percentage of stations with increasing, decreasing, statistically significant increasing, and statistically significant decreasing trends in Rx1day and Rx5day based on the Mann–Kendall test over the IPCC AR6 reference regions during the 1900–2018 period. Values higher than the upper 97.5th percentile from the 1000 bootstrap realizations under the no-trend null hypothesis are shown in boldface. There are no regions in which the percentage values lie below the lower 2.5th percentile of these bootstrap distributions.

		Rx1day				Rx5day			
Region name	No. of stations	Increase (%)	Decrease (%)	Significant increase (%)	Significant decrease (%)	Increase (%)	Decrease (%)	Significant increase (%)	Significant decrease (%)
Northwest North America (NWN)	40	57.5	42.5	5.0	10.0	57.5	42.5	**15.0**	0.0
Western North America (WNA)	78	61.5	38.5	**14.1**	2.6	61.5	38.5	**12.8**	3.8
Central North America (CNA)	126	**79.4**	20.6	**21.4**	0.8	**81.0**	19.0	**11.9**	1.6
Eastern North America (ENA)	120	**72.5**	27.5	**13.3**	2.5	**79.2**	20.8	**14.2**	1.7
Northern South America (NSA)	62	56.5	43.5	4.8	3.2	25.8	74.2	1.6	16.1
Northern Europe (NEU)	314	**79.9**	20.1	**22.0**	0.6	**90.1**	9.9	**38.5**	0.3
Western and central Europe (WCE)	323	**72.8**	27.2	**18.0**	0.3	**76.8**	23.2	**25.4**	1.5
Eastern Europe (EEU)	54	**88.9**	11.1	**38.9**	0.0	**88.9**	11.1	**46.3**	0.0
Mediterranean (MED)	82	57.3	42.7	**12.2**	3.7	54.9	45.1	**15.9**	3.7
West Southern Africa (WSAF)	64	71.9	28.1	9.4	0.0	76.6	23.4	9.4	1.6
East Southern Africa (ESAF)	79	73.4	26.6	**13.9**	1.3	65.8	34.2	**13.9**	0.0
Eastern Siberia (ESB)	45	**84.4**	15.6	**42.2**	0.0	**86.7**	13.3	**35.6**	0.0
Southeast Asia (SEA)	329	62.3	37.7	**11.9**	**10.3**	68.1	31.9	**25.8**	8.2
Southern Australia (SAU)	78	48.7	51.3	5.1	5.1	41.0	59.0	1.3	5.1

with that which would be expected from the null hypothesis of no trend.

For the 1900–2018 period using 1974 stations, the estimated precipitation sensitivities of Rx1day and Rx5day to GMST increase are 5.5% K^{-1} (4.8%–7.5% K^{-1}) and 6.3% K^{-1} (4.9%–7.5% K^{-1}), respectively. They are comparable with that for the 1950–2018 period and Westra et al. (2013), indicating that the analysis period does not have a substantial effect on the scaling relationship between annual maximum precipitation and GMST on a global scale.

The addition of 9 years of data since 2010 increases the fraction of stations with significant positive trends while the percentage of stations with significant negative trends remains unchanged and consistent with what would be expected under the null hypothesis of no trend. This is the case for long-term stations that have sufficient data for trend analysis over 1900–2018 but have relatively confined spatial distribution and for the shorter time period 1950–2018 when spatial coverage of data is much improved. It is clear that the signal of extreme precipitation intensification is more detectable with additional records, which may due to the higher power of detection that results from using longer records (Zhang et al. 2004).

To help interpret these findings we produced 1000 Monte Carlo simulations of annual extremes for the period 1950–2018 by sampling from the nonstationary GEV distributions described in section 2 that were fitted at each station. Mann–Kendall trend analysis was conducted on the simulated time series of annual extremes. The percentage of stations with significantly increasing trends during 1950–2018 is always larger than that over 1950–2009, indicating a larger power of detection when the data since 2010 are added. The observed difference in fraction of stations with significant trends in Rx1day between the periods 1950–2009 and 1950–2018 is also consistent with that due to the sample size increases by nine years. Thus while low-frequency climate variability could have contributed to higher rates of detection when recent data are included, it seems more likely that this is the result of the enhancement statistical power of trend detection for longer records.

4. Conclusions and discussion

We have analyzed trends in the annual maximum amount of precipitation accumulated in 1 day (Rx1day) and in 5 consecutive days (Rx5day) over global land areas for which we have access to station observations. We have also analyzed the relation between annual maximum precipitation and GMST.

Our analyses are conducted for two time periods, over 1950–2018 when we have the best spatial coverage and over 1900–2018 when we have longer station records (i.e., better temporal coverage) but much more limited spatial coverage. Rx1day and Rx5day have both intensified significantly at the global and continental scales, as well as in many large regions. For the period 1950–2018, close to two-thirds of stations show increasing trends, with about 9.1% and 10.9% of stations showing statistically significant increasing trends for Rx1day and Rx5day, respectively, based on a nonparametric trend test that is expected to falsely detect increasing trends 2.5% of the time. These percentages are significantly greater than 2.5%, indicating evidence for broad and systematic change in the intensity of extreme precipitation. This same test shows significant decreasing trends at rates that are consistent with the 2.5% false detection rate, indicating that the test performs as expected in the absence of processes that would be expected to weaken extreme precipitation over time in land areas with observations. This latter result also indicates that any departures from the assumption of serial independence that is made when applying the test do not produce spurious significant trends. For the period 1900–2018, more than two-thirds of stations show increasing trends with the percentage of stations showing significant increasing trends double that in 1950–2018. On the other hand, the percentages of stations with significant decreasing trends are again small and consistent with the expected false detection rate.

Intensification of extreme precipitation is evident throughout global land areas for which station data are available; stations with significant increasing trends are not limited to specific geographic locations but are widespread. At the continental scale, a significant intensification of extreme precipitation has been observed in well-gauged continental areas including Europe, Asia, and North America. Uncertainty in the characterization of changes in precipitation extremes is higher in continents where data coverage is poor including Africa, South America, and Australasia due to sparse station coverage and nonrepresentative spatial sampling. It appears that increases in extreme precipitation dominate in both Africa and South America over areas with data coverage. At the regional scale, detection of significant trends becomes more difficult as the signal-to-noise ratio decreases. Nevertheless, statistically significant intensification in extreme precipitation is still observed in many regions, including central and eastern North America, northern Central America, northern Europe, the Russian Far East, eastern central Asia, and East Asia, whereas an obvious decreasing trend in Rx5day is observed in southern Australia.

Fitting Rx1day and Rx5day to GEV distributions with GMST as a covariate reveals a significant association between changes in extreme precipitation and temperature. The connection is again statistically significant at the global scale, as it is in three continents and many regions where precipitation data are more abundant. The median estimated sensitivity of extreme precipitation to warming over the global land areas with station data is 6.6% (5.1% to 8.2%; 5%–95% confidence interval) and 5.7% (5.0% to 8.0%) per 1 K of temperature increase for Rx1day and Rx5day, respectively. These scaling rates are broadly consistent with the expected increase in the water holding capacity of the atmosphere governed by the Clausius–Clapeyron relation. Estimated scaling rates are more uncertain for records that are less complete, but do not seem to be greatly influenced by the timing of the missing years in the indices records. Nevertheless, the sensitivity of extreme precipitation to warming can differ substantially from these median values regionally, both because circulation change may be an important factor in some regions and because GMST change may not be a good indicator of regional changes in atmospheric water holding capacity. Warming over global land

is typically larger than that of GMST due to differences in sensible heat production over land and ocean surfaces. As a result, extreme precipitation sensitivity is generally smaller over land than predicted by the Clausius–Clapeyron relation if local or regional temperature change is used in the estimation, except in some tropical convergence regions. Yet, it is unclear what is the most appropriate temperature for the purpose of estimating the sensitivity (Trenberth et al. 2015).

While our results are generally consistent with those of Westra et al. (2013), the extent to which direct comparison can be made is limited because of different selections of stations in the two analyses and also because we have used more stringent criteria for retaining stations for analysis in our study. We compared our analyses with data ending in year 2018 with analyses using data ending 2009 and found, with the additional 9 years of data, that a larger percentage of stations show significant increases in extreme precipitation but that there is effectively no change in the number of stations showing significant decreases. We showed that this increase is consistent with the expected increase in detection power that should result from the availability of records that are nine years longer in the context of a warming climate. Based on the results presented here, the findings of extreme precipitation intensification over land by Westra et al. (2013) appear robust.

Although the distribution of trends across space is very noisy, our results do exhibit some spatial structure at the regional scale, such as a weakening of extreme precipitation in the Canadian Prairies, some parts of the western United States, Australia, and northern China. This suggests that other factors, such as changes in atmospheric circulation, oceanic oscillations, and aerosols may also have influenced regional trends in extreme precipitation to some extent. For instance, the decline of the Asian monsoonal circulation strength that has been related to aerosols may have contributed to the regionally coherent pattern of decreasing trends in extreme precipitation in northern China (Wang and Zhou 2005; You et al. 2011). Decreasing extreme precipitation over the Canadian Prairies may be connected with low-frequency atmospheric, oceanic oscillations, and snowfall decreases (Vincent et al. 2015; Yang et al. 2019). Atmospheric circulation change and low-frequency modes of variability have also been implicated in changes in southern Australian precipitation (Li et al. 2012; Dey et al. 2019). Changes in the subtropical ridge (Timbal and Drosdowsky 2013; Whan et al. 2014) and the southern annular mode (Cai et al. 2011; Thompson et al. 2011) were shown as potential drivers for the decline in extreme precipitation in parts of Australia. Despite the considerable research in this area, the causes of these variations are not fully understood. The association between large-scale circulation anomalies, aerosols, and changes in non-well-mixed GHGs such as ozone and changes in extreme precipitation events therefore requires further investigation.

We conclude by pointing out some caveats to our analysis. While we have used an area weighting scheme that should ensure that statistics are representative of the global land area that is sampled by the available observing networks, their uneven and incomplete spatial coverage means that our results may not be fully representative of the global land surface average of extreme changes. In particular, we note that the vast majority of stations are in the midlatitudes of the Northern Hemisphere. Tropical, subtropical, and midlatitude Southern Hemispheric areas are much less well sampled, and there is a dearth of observations in regions where projections (e.g., Kharin et al. 2013) suggest declines in future precipitation extremes. There remains an urgent need to improve data collection in regions in which the stations records are limited, especially subtropical and tropical regions, Africa, and South America, to better constrain changes in extreme precipitation.

Another caveat is that while we have attempted to use data that have been systematically quality controlled, the data quality remains a concern. Precipitation measurements are difficult to homogenize due to their high spatial and temporal variability. Thus the data we use are likely not free of inhomogeneities from, for example, changes in the type of instrumentation used to measure precipitation since different rain gauges have different wind undercatch, wetting losses, and evaporation losses (Metcalfe et al. 1997). Automatic gauges, which have different recording characteristics than the gauges that they have replaced (WMO 2017), have been widely adopted owing to the cost of manual or mechanically recorded gauges together with the development of electronic recording gauges (Kidd et al. 2017). The adoption of these gauges has no doubt induced inhomogeneities in the precipitation data we analyze that for the moment are unavoidable since the exclusion of data from automated stations would result in extremely limited global coverage in recent decades (Kidd et al. 2017). However, we were careful to focus on data that have previously been assessed to be of high quality and, in some cases, have been adjusted to improve homogeneity. As inhomogeneities are unlikely to be systematic globally, our results should hold.

While these are important caveats, we reiterate that the preponderance of evidence from the available global collection of well-studied long records of observed daily precipitation amounts indicates that precipitation extremes are intensifying in most observed regions and on a global scale, and that these changes appear to be consistent with the warming that has been observed over the same period. Moreover, this evidence, which is also supported by formal detection and attribution analyses (Min et al. 2011; Zhang et al. 2013; Li et al. 2017; Dong et al. 2020, Kirchmeier-Young and Zhang 2020; Paik et al. 2020), has strengthened somewhat with the additional observations that have accumulated over the past 9 years.

Acknowledgments. The study was supported by the Pan-Canadian Global Water Futures (GWF) research program. We acknowledge the European Climate Assessment Dataset project, the Southeast Asian Climate Assessment and Dataset project, the Latin American Climate Assessment and Dataset project, the National Climatic Data Center, the CCl/WCRP/JCOMM Expert Team on Climate Change Detection and Indices (ETCCDI), the China Meteorological Administration, the Russian Met Service, and the Australian Bureau of Meteorology for providing observational data. LVA is funded by the Australian Research Council Grant CE170100023.

REFERENCES

Aguilar, E., and Coauthors, 2009: Changes in temperature and precipitation extremes in western central Africa, Guinea Conakry, and Zimbabwe, 1955–2006. *J. Geophys. Res.*, **114**, D02115, https://doi.org/10.1029/2008JD011010.

Alexander, L. V., and J. M. Arblaster, 2017: Historical and projected trends in temperature and precipitation extremes in Australia in observations and CMIP5. *Wea. Climate Extreme*, **15**, 34–56, https://doi.org/10.1016/J.WACE.2017.02.001.

——, and Coauthors, 2006: Global observed changes in daily climate extremes of temperature and precipitation. *J. Geophys. Res.*, **111**, D05109, https://doi.org/10.1029/2005JD006290.

Allen, M. R., and W. J. Ingram, 2002: Constraints on future changes in climate and the hydrologic cycle. *Nature*, **419**, 228–232, https://doi.org/10.1038/NATURE01092.

Asadieh, B., and N. Y. Krakauer, 2015: Global trends in extreme precipitation: Climate models versus observations. *Hydrol. Earth Syst. Sci.*, **19**, 877–891, https://doi.org/10.5194/HESS-19-877-2015.

Barbero, R., H. J. Fowler, G. Lenderink, and S. Blenkinsop, 2017: Is the intensification of precipitation extremes with global warming better detected at hourly than daily resolutions? *Geophys. Res. Lett.*, **44**, 974–983, https://doi.org/10.1002/2016GL071917.

Blöschl, G., R. Merz, J. Parajka, J. Salinas, and A. Viglione, 2012: Floods in Austria. *Changes in Flood Risk in Europe*, Z. W. Kundzewicz, Ed., IAHS Special Publication, 169–177.

Boer, G. J., 1993: Climate change and the regulation of the surface moisture and energy budgets. *Climate Dyn.*, **8**, 225–239, https://doi.org/10.1007/BF00198617.

Caesar, J., and Coauthors, 2011: Changes in temperature and precipitation extremes over the Indo-Pacific region from 1971 to 2005. *Int. J. Climatol.*, **31**, 791–801, https://doi.org/10.1002/JOC.2118.

Cai, W., P. Van Rensch, S. Borlace, and T. Cowan, 2011: Does the Southern Annular Mode contribute to the persistence of the multidecade-long drought over southwest Western Australia? *Geophys. Res. Lett.*, **38**, L14712, https://doi.org/10.1029/2011GL047943.

Contractor, S., M. G. Donat, and L. V. Alexander, 2018: Intensification of the daily wet day rainfall distribution across Australia. *Geophys. Res. Lett.*, **45**, 8568–8576, https://doi.org/10.1029/2018GL078875.

Dey, R., S. C. Lewis, J. M. Arblaster, and N. J. Abram, 2019: A review of past and projected changes in Australia's rainfall. *Wiley Interdiscip. Rev.: Climate Change*, **10**, e577, https://doi.org/10.1002/WCC.577.

Donat, M. G., L. V. Alexander, H. Yang, I. Durre, R. Vose, and J. Caesar, 2013a: Global land-based datasets for monitoring climatic extremes. *Bull. Amer. Meteor. Soc.*, **94**, 997–1006, https://doi.org/10.1175/BAMS-D-12-00109.1.

——, and Coauthors, 2013b: Updated analyses of temperature and precipitation extreme indices since the beginning of the twentieth century: The HadEX2 dataset. *J. Geophys. Res. Atmos.*, **118**, 2098–2118, https://doi.org/10.1002/JGRD.50150.

——, and Coauthors, 2014: Changes in extreme temperature and precipitation in the Arab region: Long-term trends and variability related to ENSO and NAO. *Int. J. Climatol.*, **34**, 581–592, https://doi.org/10.1002/JOC.3707.

——, A. L. Lowry, L. V. Alexander, P. A. O'Gorman, and N. Maher, 2016: More extreme precipitation in the world's dry and wet regions. *Nat. Climate Change*, **6**, 508–513, https://doi.org/10.1038/nclimate2941..

Dong, S., Y. Sun, and C. Li, 2020: Detection of human influence on precipitation extremes in Asia. *J. Climate*, **33**, 5293–5304, https://doi.org/10.1175/JCLI-D-19-0371.1.

Dunn, R. J. H., and Coauthors, 2020: Development of an updated global land in-situ-based dataset of temperature and precipitation extremes: HadEX3. *J. Geophys. Res. Atmos.*, **125**, e2019JD032263, https://doi.org/10.1029/2019JD032263.

Groisman, P. Ya., R. W. Knight, D. R. Easterling, T. R. Kar, G. C. Hegerl, and V. A. N. Razuvaev, 2005: Trends in intense precipitation in the climate record. *J. Climate*, **18**, 1326–1350, https://doi.org/10.1175/JCLI3339.1.

Hansen, J., R. Ruedy, M. Sato, and K. Lo, 2010: Global surface temperature change. *Rev. Geophys.*, **48**, RG4004, https://doi.org/10.1029/2010RG000345.

Hartmann, D. L., and Coauthors, 2013: Observations: Atmosphere and surface. *Climate Change 2013: The Physical Science Basis*, T. F. Stocker et al., Eds., Cambridge University Press, 159–254.

Hope, P. K., 2006: Projected future changes in synoptic systems influencing southwest Western Australia. *Climate Dyn.*, **26**, 765–780, https://doi.org/10.1007/S00382-006-0116-X.

IPCC, 2012: *Managing the Risks of Extreme Events and Disasters to Advance Climate Change Adaptation*. C. B. Field et al., Eds., Cambridge University Press, 582 pp.

——, 2013: *Climate Change 2013: The Physical Science Basis*. T. F. Stocker et al., Eds., Cambridge University Press, 1535 pp., https://doi.org/10.1017/CBO9781107415324.

——, 2018: Global warming of 1.5°C: An IPCC Special Report on the impacts of global warming of 1.5°C above pre-industrial levels and related global greenhouse gas emission pathways, in the context of strengthening the global response to the threat of climate change, sustainable development, and efforts to eradicate poverty. V. Masson-Delmotte et al., Eds., Cambridge University Press, https://www.ipcc.ch/sr15/.

Iturbide, M., and Coauthors, 2020: An update of IPCC climate reference regions for subcontinental analysis of climate model data: Definition and aggregated datasets. *Earth Syst. Sci. Data Discuss.*, https://doi.org/10.5194/essd-2019-258.

Jones, M. R., H. J. Fowler, C. G. Kilsby, and S. Blenkinsop, 2013: An assessment of changes in seasonal and annual extreme rainfall in the UK between 1961 and 2009. *Int. J. Climatol.*, **33**, 1178–1194, https://doi.org/10.1002/JOC.3503.

Kharin, V. V., F. W. Zwiers, X. Zhang, and M. Wehner, 2013: Changes in temperature and precipitation extremes in the CMIP5 ensemble. *Climatic Change*, **119**, 345–357, https://doi.org/10.1007/S10584-013-0705-8.

Kidd, C., A. Becker, G. J. Huffman, C. L. Muller, P. Joe, G. Skofronick-Jackson, and D. B. Kirschbaum, 2017: So, how much of the Earth's surface is covered by rain gauges? *Bull. Amer. Meteor. Soc.*, **98**, 69–78, https://doi.org/10.1175/BAMS-D-14-00283.1.

Kiktev, D., D. M. Sexton, L. V. Alexander, and C. K. Folland, 2003: Comparison of modeled and observed trends in indices of daily climate extremes. *J. Climate*, **16**, 3560–3571, https://doi.org/10.1175/1520-0442(2003)016<3560:COMAOT>2.0.CO;2.

King, A. D., L. V. Alexander, and M. G. Donat, 2013: Asymmetry in the response of eastern Australia extreme rainfall to low-frequency Pacific variability. *Geophys. Res. Lett.*, **40**, 2271–2277, https://doi.org/10.1002/GRL.50427.

Kirchmeier-Young, M. C., and X. Zhang, 2020: Human influence has intensified extreme precipitation in North America. *Proc. Natl. Acad. Sci. USA*, **117**, 13 308–13 313, https://doi.org/10.1073/PNAS.1921628117.

Lavery, B., A. Kariko, and N. Nicholls, 1992: A historical rainfall data set for Australia. *Aust. Meteor. Mag.*, **40**, 33–39.

Li, C., F. Zwiers, X. Zhang, and G. Li, 2019: How much information is required to well constrain local estimates of future precipitation extremes? *Earth's Future*, **7**, 11–24, https://doi.org/10.1029/2018EF001001.

Li, H., H. Chen, and H. Wang, 2017: Effects of anthropogenic activity emerging as intensified extreme precipitation over China. *J. Geophys. Res. Atmos.*, **122**, 6899–6914, https://doi.org/10.1002/2016JD026251.

Li, J. P., J. Feng, and Y. Li, 2012: A possible cause of decreasing summer rainfall in northeast Australia. *Int. J. Climatol.*, **32**, 995–1005, https://doi.org/10.1002/joc.2328.

Li, W., Z. H. Jiang, X. Zhang, and L. Li, 2018: On the emergence of anthropogenic signal in extreme precipitation change over China. *Geophys. Res. Lett.*, **45**, 9179–9185, https://doi.org/10.1029/2018GL079133.

Livezey, R. E., and W. Y. Chen, 1983: Statistical field significance and its determination by Monte Carlo techniques. *Mon. Wea. Rev.*, **111**, 46–59, https://doi.org/10.1175/1520-0493(1983)111<0046:SFSAID>2.0.CO;2.

Mann, H. B., 1945: Nonparametric tests against trend. *Econometrica*, **13**, 245–259, https://doi.org/10.2307/1907187.

Mekis, É., and L. A. Vincent, 2011: An overview of the second generation adjusted daily precipitation dataset for trend analysis in Canada. *Atmos.–Ocean*, **49**, 163–177, https://doi.org/10.1080/07055900.2011.583910.

Metcalfe, J. R., B. Routledge, and K. Devine, 1997: Rainfall measurement in Canada: Changing observational methods and archive adjustment procedures. *J. Climate*, **10**, 92–101, https://doi.org/10.1175/1520-0442(1997)010<0092:RMICCO>2.0.CO;2.

Min, S. K., X. Zhang, F. W. Zwiers, and G. C. Hegerl, 2011: Human contribution to more-intense precipitation extremes. *Nature*, **470**, 378–381, https://doi.org/10.1038/nature09763.

O'Gorman, P. A., 2015: Precipitation extremes under climate change. *Curr. Climate Change Rep.*, **1**, 49–59, https://doi.org/10.1007/s40641-015-0009-3.

Paik, S., S. K. Min, X. Zhang, M. G. Donat, A. D. King, and Q. Sun, 2020: Determining the anthropogenic greenhouse gas contribution to the observed intensification of extreme precipitation. *Geophys. Res. Lett.*, **47**, e2019GL086875, https://doi.org/10.1029/2019GL086875.

Peterson, T. C., X. B. Zhang, M. Brunet-India, and J. L. Vázquez-Aguirre, 2008: Changes in North American extremes derived from daily weather data. *J. Geophys. Res.*, **113**, D07113, https://doi.org/10.1029/2007JD009453.

Raut, B. A., C. Jakob, and M. J. Reeder, 2014: Rainfall changes over southwestern Australia and their relationship to the southern annular mode and ENSO. *J. Climate*, **27**, 5801–5814, https://doi.org/10.1175/JCLI-D-13-00773.1.

Thompson, D. W., S. Solomon, P. J. Kushner, M. H. England, K. M. Grise, and D. J. Karoly, 2011: Signatures of the Antarctic ozone hole in Southern Hemisphere surface climate change. *Nat. Geosci.*, **4**, 741–749, https://doi.org/10.1038/ngeo1296.

Timbal, B., and W. Drosdowsky, 2013: The relationship between the decline of southeastern Australian rainfall and the strengthening of the subtropical ridge. *Int. J. Climatol.*, **33**, 1021–1034, https://doi.org/10.1002/joc.3492.

Trenberth, K. E., J. T. Fasullo, and T. G. Shepherd, 2015: Attribution of climate extreme events. *Nat. Climate Change*, **5**, 725–730, https://doi.org/10.1038/nclimate2657.

van den Besselaar, E. J. M., A. M. G. Klein Tank, and T. A. Buishand, 2013: Trends in European precipitation extremes over 1951–2010. *Int. J. Climatol.*, **33**, 2682–2689, https://doi.org/10.1002/joc.3619.

——, and Coauthors, 2015: International Climate Assessment & Dataset: Climate services across borders. *Bull. Amer. Meteor. Soc.*, **96**, 16–21, https://doi.org/10.1175/BAMS-D-13-00249.1.

Vincent, L. A., X. Zhang, R. D. Brown, Y. Feng, E. Mekis, E. J. Milewska, H . Wan, and X. L. Wang, 2015: Observed trends in Canada's climate and influence of low-frequency variability modes. *J. Climate*, **28**, 4545–4560, https://doi.org/10.1175/JCLI-D-14-00697.1.

Wang, Y., and L. Zhou, 2005: Observed trends in extreme precipitation events in China during 1961–2001 and the associated changes in large-scale circulation. *Geophys. Res. Lett.*, **32**, L09707, https://doi.org/10.1029/2005GL023769.

Westra, S., L. V. Alexander, and F. W. Zwiers, 2013: Global increasing trends in annual maximum daily precipitation. *J. Climate*, **26**, 3904–3918, https://doi.org/10.1175/JCLI-D-12-00502.1.

Whan, K., B. Timbal, and J. Lindesay, 2014: Linear and nonlinear statistical analysis of the impact of sub-tropical ridge intensity and position on south-east Australian rainfall. *Int. J. Climatol.*, **34**, 326–342, https://doi.org/10.1002/joc.3689.

WMO, 2017: Guide to meteorological instruments and methods of observation. WMO, 186–216, https://library.wmo.int/doc_num.php?explnum_id=3152.

Yang, Y., T. Y. Gan, and X. Tan, 2019: Spatiotemporal changes in precipitation extremes over Canada and their teleconnections to large-scale climate patterns. *J. Hydrometeor.*, **20**, 275–296, https://doi.org/10.1175/JHM-D-18-0004.1.

You, Q., and Coauthors, 2011: Changes in daily climate extremes in China and their connection to the large scale atmospheric circulation during 1961–2003. *Climate Dyn.*, **36**, 2399–2417, https://doi.org/10.1007/s00382-009-0735-0.

Zhang, X., and F. W. Zwiers, 2004: Comment on ''Applicability of prewhitening to eliminate the influence of serial correlation on the Mann-Kendall test'' by Sheng Yue and Chun Yuan Wang. *Water Resour. Res.*, **40**, W03805, https://doi.org/10.1029/2003WR002073.

——, ——, and G. Li, 2004: Monte Carlo experiments on the detection of trends in extreme values. *J. Climate*, **17**, 1945–1952, https://doi.org/10.1175/1520-0442(2004)017<1945:MCEOTD>2.0.CO;2.

——, H. Wan, F. W. Zwiers, G. C. Hegerl, and S. K. Min, 2013: Attributing intensification of precipitation extremes to human influence. *Geophys. Res. Lett.*, **40**, 5252–5257, https://doi.org/10.1002/grl.51010.

Zolina, O., 2012: Changes in intense precipitation in Europe. *Changes in Flood Risk in Europe*, Z. W. Kundzewicz, Ed., IAHS Special Publication, 97–120.